Ore Geology Reviews 106 (2019) 340–350

Contents lists available at ScienceDirect

Ore Geology Reviews

journal homepage: www.elsevier.com/locate/oregeorev

Evidence of boiling and epithermal vein mineralization in Carlin-type deposits on the Getchell trend, Nevada

John A. Groff

Department of Earth and Environmental Sciences, New Mexico Institute of Mining and Technology, 801 Leroy, Socorro, NM 87801, United States

ARTICLE INFO

Keywords:
Carlin-type gold deposits
Fluid boiling
Low-sulfidation epithermal gold deposits
Nevada

ABSTRACT

Boiling in northeast (NE)-trending faults during Eocene gold mineralization at the Getchell and Twin Creeks deposits is indicated by cogenetic liquid-rich and vapor-rich fluid inclusions. Both primary and secondary fluid inclusions in orpiment record similar evidence of boiling. However, banding in paragenetically younger calcite indicates that boiling was episodic in addition to being localized to NE-trending faults. The presence of CO_2-rich secondary fluid inclusions in fluorite from the Getchell mine is an artifact of boiling and a depth of ≤980 m is representative of the Late-stage in these Carlin-type deposits.

An ~0.5 m wide crystalline white-quartz vein in the DZ Fault, Twin Creeks mine contains cogenetic liquid-rich and vapor-rich fluid inclusions. Intergrown with the quartz is 42 Ma adularia and native gold that occurs both as disseminations within and along boundaries between quartz grains. This vein extends beyond the DZ Fault and cuts massive brown jasperoid of the HGO ore zone. The contrasting styles of mineralization (e.g., low-sulfidation epithermal versus Carlin type), crosscutting relationship, and precise adularia age provides an important constraint on the age of Carlin-type gold mineralization at the Twin Creeks mine.

1. Introduction

Gold mineralization in low-sulfidation epithermal deposits is commonly associated with boiling at temperatures of 200–300 °C and depths of ≤1.5 km (Hedenquist et al., 2000). Adularia is a typical alteration mineral and this allows for the precise dating of these deposits. Modern analogs are hot springs in New Zealand that discharge metals and flash boiling produces scales containing high concentrations of gold (Brown, 1986).

Age constraints on Carlin-type gold deposits in Nevada indicate an association with Eocene magmatism. Common trace elements are Au–Tl–As–Hg–Sb, and there are low concentrations of Ag and base metals. Fluid inclusion data and mineral textures indicate that ore-forming fluids have T_h of ~180 °C to 240 °C, salinities of ~2 to 4 wt% NaCl equiv., contain modest concentrations of CO_2 (< 4 mol%) and low concentrations of CH_4 (< 0.4 mol%), and there is no evidence of boiling or immiscibility (Cline and Hofstra, 2000; Hofstra and Cline, 2000; Lubben, 2004).

The purpose of this paper is to document assemblages of fluid inclusions that provide clear evidence of boiling during Eocene mineralization at the Getchell and Twin Creeks deposits in the Getchell trend, Nevada. Fluid inclusions in Late-stage orpiment and banded calcite containing realgar from the Getchell mine are described and compared to those in quartz–adularia–native gold veins that cut Carlin-type jasperoid ore, at the Twin Creeks mine. Microthermometric and gas analyses of fluid inclusion assemblages are used to determine the depth of boiling in these deposits.

2. Geology of the Getchell trend

The Getchell trend experienced repeated episodes of igneous and hydrothermal activity from the Mid Cretaceous to Late Eocene. Age data for argillic and sericitic alteration, coupled with multiple generations of igneous intrusions indicates the Cretaceous igneous–hydrothermal event spanned a period of 109–75 Ma (Osterberg, 1990; Groff et al., 1997; Hall et al., 2000). Base metal skarn-type mineralization containing Au ± Ag formed in association with 95 and 92 Ma intrusions (Groff et al., 1997). At the Getchell mine, U–Pb and Rb–Sr dates on 34 ± 11 Ma fluorite (Hofstra et al., 2000) and 39 ± 2.1 Ma galkhaite (Tretbar et al., 2000) indicate that the Late-stage of Carlin-type gold mineralization occurred in the Late Eocene. At the Twin Creeks gold mine, an $^{40}Ar/^{39}Ar$ date on 42.11 ± 0.43 Ma adularia associated with native gold in a quartz vein indicates that gold mineralization is about the same age (Groff et al., 1997).

The Main pit at the Getchell mine is on the eastern flank of the 92 Ma Osgood Mountains granodiorite stock and Carlin-type gold

E-mail address: johnagroff@yahoo.com.

https://doi.org/10.1016/j.oregeorev.2019.02.013
Received 13 August 2017; Received in revised form 27 January 2019; Accepted 12 February 2019
Available online 13 February 2019
0169-1368/

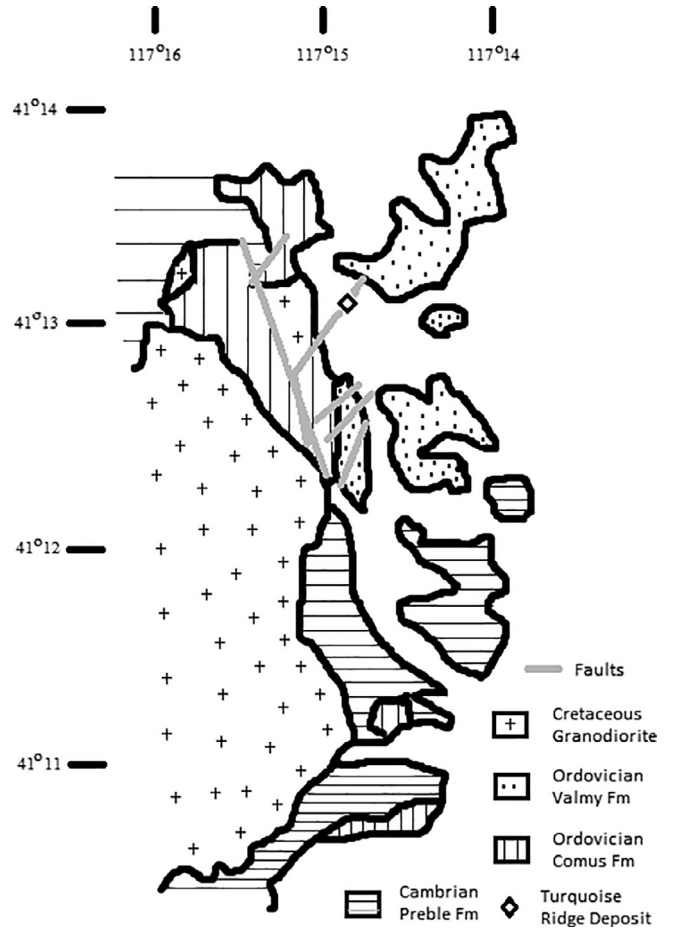

Fig. 1. Geologic map of the Getchell mine area after Cline (2001).

mineralization occurs in high-angle faults (Fig. 1). Parallel, northerly trending structures (e.g., the Getchell, Footwall, and Hanging-wall faults) in the Main pit are intersected by the NE-trending Turquoise Ridge (TRDG) Fault. Host rocks for ore include Cretaceous intrusions; the Ordovician Valmy and Comus formations; and interbedded phyllitic shale, sandstone, and limestone of the Cambrian Preble Formation that is commonly altered to a hornfels–wollastonite skarn (Madden-McGuire and Marsh, 1991; Chevillon et al., 2000). Gold was deposited by sulfidation (Cline, 2001) and there are significantly greater amounts of orpiment–realgar–calcite mineralization at the Getchell mine, compared with Twin Creeks.

Carlin-type gold mineralization at the Twin Creeks mine occurs dominantly in a northerly trending overturned anticline (Fig. 2). Host rocks for ore in the Megapit are interbedded silty shale, limestone, and mafic igneous rocks of the Ordovician Valmy and Comus formations (Fortuna et al., 2003). The Pennsylvanian–Permian Etchart Limestone hosts ore in the north section of the mine. Although NE-trending faults served as conduits for auriferous fluids, ore zones occur in favorable stratagraphic horizons containing ferroan dolomite and sulfidation is responsible for gold deposition (Stenger et al., 1998).

Late-stage minerals are macroscopic and consist of the assemblage orpiment–realgar–calcite–pyrite–stibnite–quartz–gold–adularia. These minerals occur as veins, open-space fillings and the matrix to breccia containing clasts of Main-stage ore. An overlapping sequence of mineralization consists of orpiment–pyrite, calcite–realgar–pyrite, and stibnite–pyrite–quartz–adularia (Groff, 2018a,b). Auriferous pyrite is intergrown with stibnite and occurs as fine disseminations in orpiment.

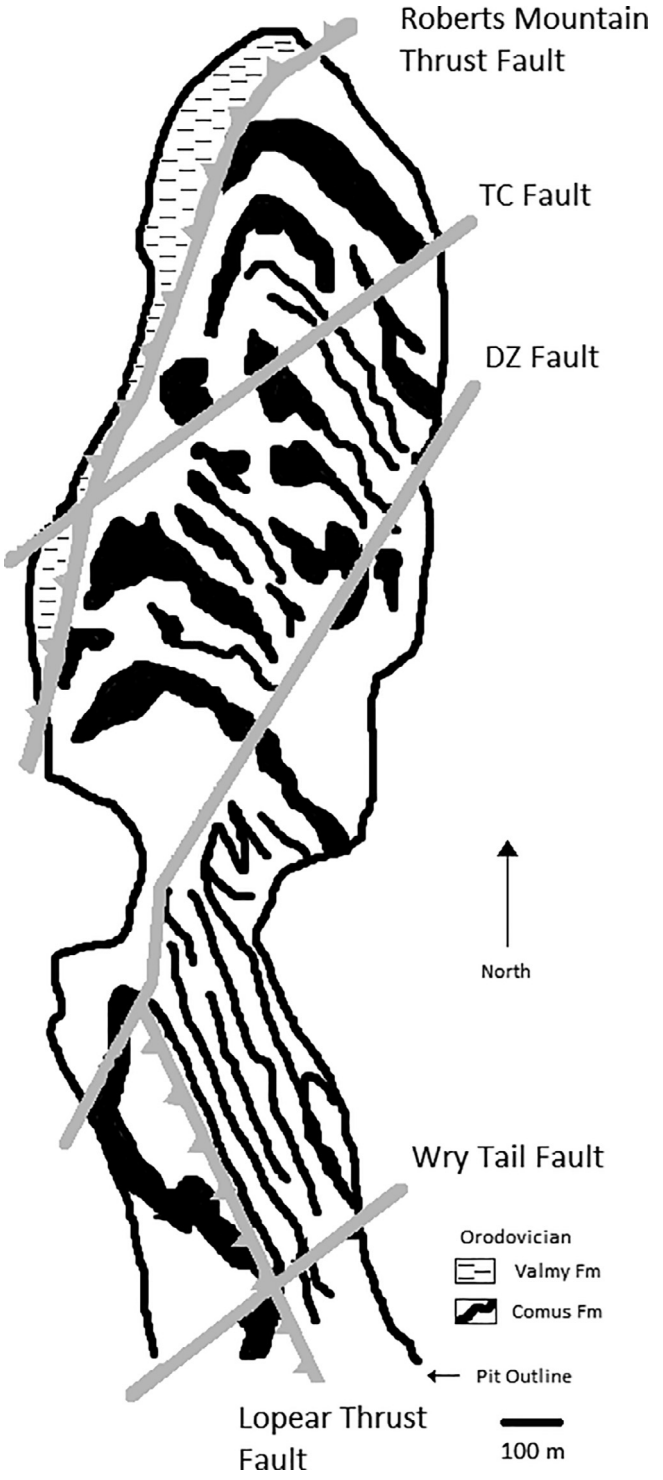

Fig. 2. A generalized geologic map of the Mega pit, Twin Creeks mine showing major faults and folding in the Ordovician Comus Formation. After Stenger et al. (1998) and Fortuna et al. (2003).

3. Samples and methods

Sixteen samples of orpiment and/or calcite containing realgar from the Main and North pits, Getchell mine were selected for fluid inclusion studies (Table 1). These samples were collected in north (N)-trending faults, the NE-trending TRDG Fault, and at structural intersections. Fluid inclusion microthermometric results are supported by quadrupole mass spectrometer (QMS) analyses of gas released by crushing of

Table 1
Descriptions of orpiment, calcite, realgar, and quartz samples used for fluid inclusion study. Abbreviations: Flt = fault, qtz = quartz, (G) = Getchell mine and (TC) = Twin Creeks mine.

Sample ID	Location	Au grade (ppm)	Fluid inclusion type(s)	Structures(s)	Description
DZADUL	Megapit (TC)	> 30	Liquid rich and vapor rich	DZ Flt	Qtz vein containing native Au and 42 Ma adularia that cuts Carlin-type ore
92–113/155	N. pit (G)	9.3	Liquid rich and vapor rich	Intersection of NE Flt and Footwall Flt	* Orpiment intergrown with realgar and banded calcite in skarn
NP775	N. pit (G)	≥ 4.5	Liquid rich and vapor rich	Getchell Flt	Fractured qtz with fillings of orpiment and realgar
NPSTOPE	N. pit (G)	≥ 4.5	Liquid rich	Intersection of NE Flt and Footwall Flt	Mass of banded calcite intergrown with realgar, orpiment, and purple fluorite in historic stope
NP782	N. pit (G)	4.6	Liquid rich	Footwall Flt	Bands of intergrown orpiment, realgar, and clear calcite on bedding planes in skarn
92–225/1126	Main pit (G)	3.7	and vapor rich	Intersection of TRDG and Footwall flts	** Orpiment intergrown with realgar and banded calcite in skarn
99–1550	Main pit (G)	4.6	Liquid rich and vapor rich	TRDG Flt	Vein of banded calcite, containing realgar, cuts silicified granodiorite
#21	Main pit (G)	6.9	Liquid rich and vapor rich	TRDG Flt	Orpiment vein, 2 m wide
#19	Main pit (G)	6.0	Liquid rich and vapor rich	Intersection of TRDG and Hanging-wall flts	Jasperoid with fracture and vug fillings of orpiment and clear fluorite
91–165/800	Main pit (G)	0.5	Liquid rich	Footwall Flt	Orpiment vein, 1.5 m wide
92–205/1080	Main pit (G)	21.3	Liquid rich	Footwall Flt	Silicified black shale with vug and fracture fillings of coarse orpiment and realgar crystals
#7	Main pit (G)	4.7	Liquid rich and vapor rich	Extension of TRDG Flt from the Getchell Flt	Orpiment vein, 1 m wide, with fine realgar on the vein margin and along partings in opriment
#10	Main pit (G)	21.0	Liquid rich	Footwall Flt	Bands of intergrown orpiment, realgar, and clearcalcite on bedding planes in skarn
#35	Main pit (G)	4.6	Liquid rich	Getchell Flt	Breccia with siliceous–pyritic matrix that contains orpiment and realgar crystals along fractures
#12	Main pit (G)	5.1	Liquid rich	Getchell Flt	Orpiment– realgar– stibnite open-space fillings
92–198/318	Main pit (G)	33.0	Liquid rich	Extension of TRDG Flt from the Getchell Flt	Massive orpiment with fine realgar rimming individual orpiment crystals
#14	Main pit (G)	60.0	Liquid rich	Footwall Flt	Bands of orpiment and realgar on bedding planes in skarn

* 11 mol% CO2 determined by QMS gas analyses.
** 10.2 mol% CO2 determined by QMS gas analyses.

orpiment, realgar, and quartz separates from both the Getchell and Twin Creeks mines.

3.1. Petrography

No samples of orpiment, calcite, and realgar were cut or polished prior to petrographic study. Orpiment and calcite were cleaved with a razor blade to produce ~1.5 mm to 3 mm thick sections. Whereas transparent realgar crystals were handpicked from samples. Multiple realgar crystals or sections of orpiment and calcite for each sample were studied to determine fluid inclusion populations.

A crystalline white-quartz vein (~0.3-m wide) that originates in the NE-trending DZ Fault, Twin Creeks mine and contains native gold with 42 Ma adularia was sampled over a 21 cm length (Table 1). Doubly polished sections (2–4 mm thick) were prepared at 7 cm increments along the quartz vein.

3.2. Microthermometry and gas analyses

Fluid inclusion heating and freezing analyses were conducted on a Linkham Th 600 stage (precision of ± 0.1 °C) housed at the New Mexico Institute of Mining and Technology. Calibration of the stage was completed using commercial standards (with different melting points), distilled water, and laboratory-created chips containing fluid inclusions of pure water and CO_2. The presence, or absence, of CO_2-rich fluid inclusions in samples was determined by petrography and freezing analyses.

A Balzer 420 quadrupole mass spectrometer (QMS) housed at the New Mexico Institute of Mining and Technology was used to measure fluid inclusion volatiles released by in-vacuo crushing at room temperature (Groff, 2018b). Measurements by the QMS were made every 100–200 ms for gas species including H_2O, CO_2, CH_4, N_2, Ar, and hydrocarbons (C_nH_m). Orpiment and realgar crystals were handpicked from pit samples and drill core; studied using a binocular microscope to ensure purity of the separate; and triple rinsed with hydrochloric acid and distilled water. Quartz from a pit sample of the DZ Fault was cleaned using hydrochloric acid and NaOH; then boiled in distilled water for 30 minutes. All samples were placed in a low-temperature oven overnight to dry. Prior to analysis using the crush-fast-scan method (Norman et al., 1996), samples were under vacuum for 12 h to remove adsorbed gases.

4. Fluid inclusion studies

4.1. Petrography

Fluid inclusions in samples of orpiment from the Getchell and Twin Creeks mines are liquid-rich (< 20% vapor), with a small population (≤10%) of one-phase liquid-only inclusions (Groff, 1996). However, the results of the present study indicate that samples from a NE-trending structure in the North pit (e.g., 92–113 and NPSTOPE; Table 1) and the NE-trending TRDG Fault (e.g., #7 and #21; Table 1), Getchell mine contain cogenetic liquid-rich and vapor-rich (> 50% vapor) inclusions (Table 1). This assemblage is present as both primary and secondary inclusions (Fig. 3a, b), based on the criteria established by Roedder (1984).

At the Getchell mine, samples of calcite intergrown with realgar in a NE-trending structure (e.g., NPSTOPE and 99–1550; Table 1), display millimeter-scale banding (Fig. 4a). Clear bands of calcite contain sparse liquid-rich (< 20% vapor) inclusions, with consistent phase ratios (Fig. 4b). In contrast, milky bands contain an abundance of cogenetic liquid-rich and vapor-rich (> 50% vapor) inclusions (Fig. 4c). Samples beyond these structures lack banding and consist entirely of clear calcite. Fluid inclusions in realgar are almost entirely one-phase liquid (Fig. 5).

At the Twin Creeks mine, an ~0.5 m wide crystalline white-quartz

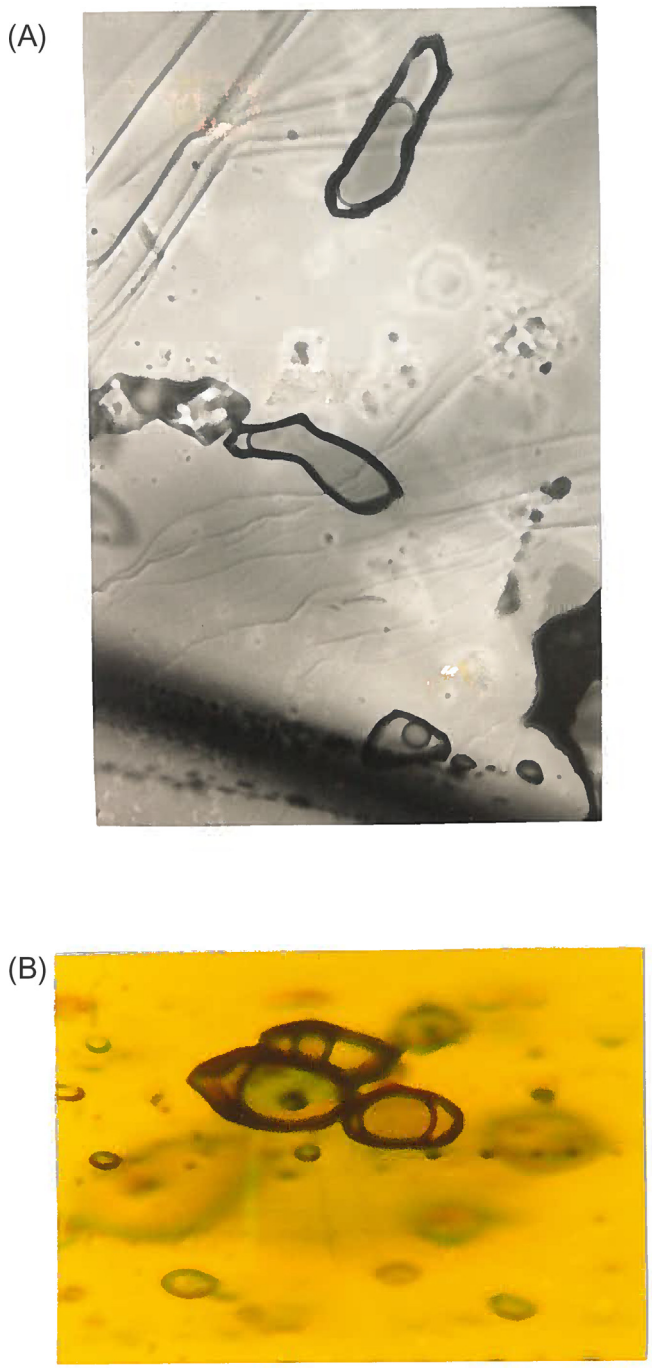

Fig. 3. Boiling recorded by (a) primary (~15 to 20 μm) and (b) secondary (~10 to 15 μm) fluid inclusions in orpiment sample #21 (Table 1), Getchell mine. The primary liquid-rich inclusion (partially obscured by the dark band near the bottom of the photomicrograph) and the vapor-rich inclusion (center of the photomicrograph) homogenize to the liquid and vapor phases at 178 °C and 180 °C, respectively.

vein contains intergrown 42 Ma adularia in the NE-trending DZ Fault (Groff et al., 1997). Native gold is disseminated in quartz grains that host primary fluid inclusions that are liquid-rich (< 20% vapor; Fig. 6a) and vapor-rich (> 50% vapor; Fig. 6b). Dark one-phase inclusions that did not change with freezing to –200 °C could be entirely vapor, or potentially leaked after trapping. Native gold grains occur within and between quartz grains that also contain assemblages of cogenetic vapor-rich and liquid-rich inclusions (Fig. 6c). Subhedral–euhedral crystals of pyrite ≤2 mm in size also occur within and between quartz crystals.

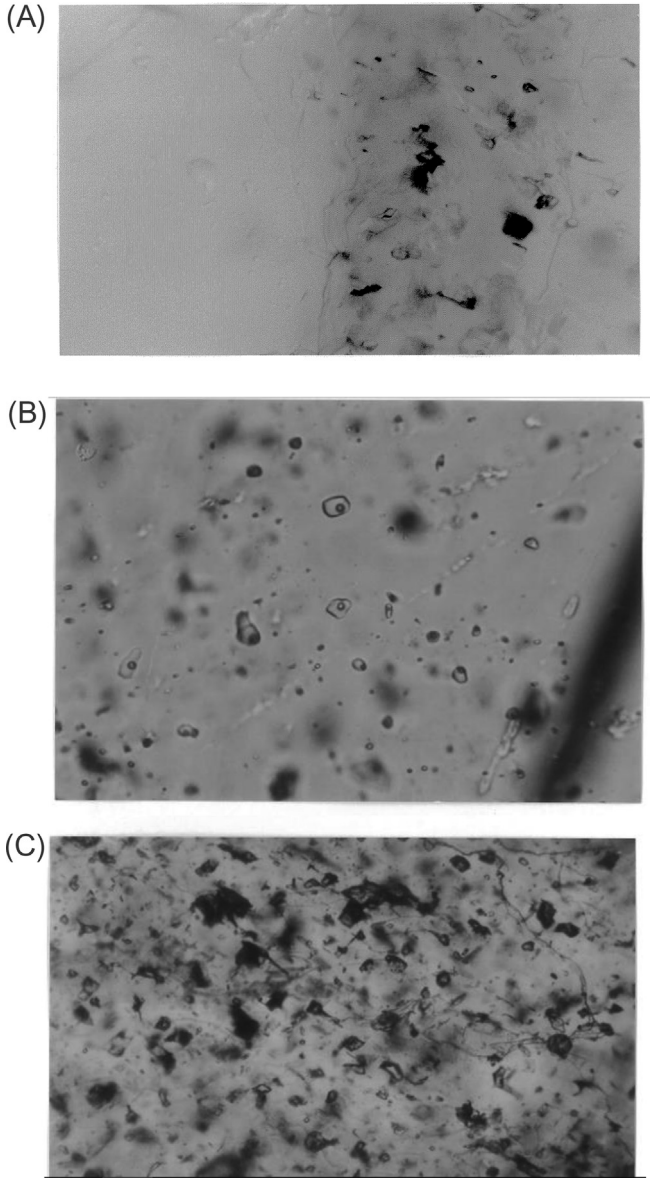

Fig. 4. Banded calcite intergrown with purple fluorite and realgar in the sample NPSTOPE (Table 1), Getchell mine. A) Bands (~1 to 3 mm) of mottled calcite and clear calcite. B) Close up of a clear band containing a low density of ~10 to 20 μm liquid-rich fluid inclusions. C) Close up of a mottled band showing a high density of ~10 to 20 μm vapor-rich and liquid-rich inclusions.

This quartz vein cuts across brown jasperoid of the HGO ore zone.

4.2. Microthermometry of fluid inclusion assemblages

Homogenization temperatures (T_h) of fluid inclusions in orpiment, calcite, realgar, and quartz could be repeated to within 1 °C. However, decrepitation of inclusions in orpiment was a problem and visible deformation occurred around primary and secondary vapor-rich inclusions with heating. Therefore, data for assemblages of cogenetic liquid-rich and vapor-rich inclusions are limited to three samples. Inclusions in the same field of view have T_h(V) 197 °C and T_h(L) 203 °C (sample 92–225, Table 1); T_h(V) 180 °C and T_h(L) 178 °C (sample #21, Fig. 3a); and Th (V) 173 °C and Th(L) 178 °C (sample #19).

The freezing of orpiment and realgar samples caused modification of some fluid inclusions. A sudden expansion occurred with the formation of ice that stretched inclusions, as evidenced by larger vapor bubbles at room temperature. One-phase liquid inclusions in realgar

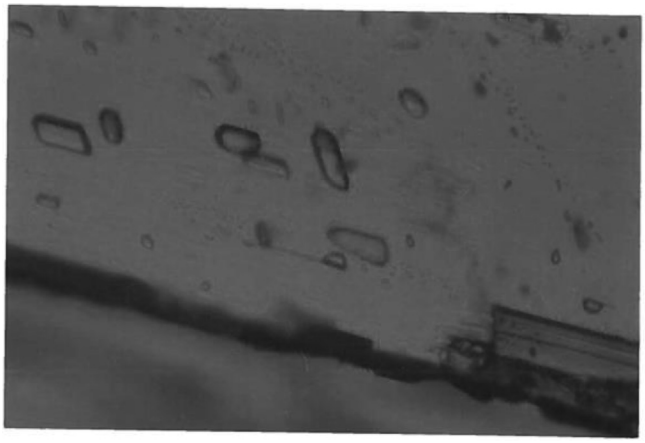

Fig. 5. Photomicrograph of 15–25 μm one-phase liquid inclusions in realgar sample #35 (Table 1), Getchell mine.

were most susceptible to stretching and many leaked with heating.

Microthermometric data were generated for primary and secondary fluid inclusions in orpiment from N- and NE-trending structures at the Getchell mine. A significant population of primary inclusions have T_h of 140–200 °C and salinity of 4–6 wt% NaCl equiv. (Fig. 7a, b). However, only inclusions in the NE-trending TRDG Fault record T_h > 200 °C and salinity > 8 wt% NaCl equiv.

Secondary fluid inclusions in orpiment have broader ranges in T_h and salinity (Fig. 7c, d). Data for the TRDG Fault form a bimodal population with T_h of 120–160 °C and 180–200 °C compared with salinities of 4–8 wt% NaCl equiv. and 12–14 wt% NaCl equiv., respectively.

Microthermometric data for banded calcite were generated for samples 99–1550 (clear bands) and NPSTOPE (mottled bands). Primary fluid inclusions in mottled bands have T_h of 140–160 °C and the highest salinities of 8–10 wt% NaCl equiv. (Fig. 8a–d). A single, primary inclusion containing a small vapor bubble in realgar sample NPSTOPE yielded T_h of 75 °C (Fig. 8a), but it ruptured upon freezing.

Microthermometric data for the 42 Ma quartz–adularia–gold vein record higher T_h compared with samples of Late-stage Carlin-type mineralization. Primary liquid-rich inclusions have Th of 206–330° (Fig. 9). Homogenization to the vapor phase could not be observed due to poor optics and inclusion shapes that lacked narrow reentrants to trap small amounts of liquid.

No CO_2-rich fluid inclusions were identified during petrography or freezing analyses of orpiment, calcite, realgar, and quartz samples. Final ice melting occurred below 0 °C and eutectic temperatures (T_e) of −21 °C were recorded, except for samples of orpiment from the TRDG Fault that yielded T_e to −25 °C.

4.3. Gas analyses of fluid inclusion extracts

Orpiment samples from the Getchell and Twin Creeks mines represent two styles of mineralization. At the Getchell mine, orpiment was collected from N- and NE- trending faults, or at structural intersections. In contrast, orpiment occurs in bedding replacement ore between NE-trending faults at the Twin Creeks mine. Fluid inclusions that contain the highest amounts of CO_2 (11 mol%) and total gases (12.1 mol%; Appendix 1) occur in samples from the intersection of the N-trending Footwall Fault and NE-trending faults, Getchell mine (Fig. 10). Beyond these intersections and in N-trending faults, the total gas contents of inclusions are commonly between 2 and 4 mol% (Fig. 10). Fluid inclusions in bedding replacement ore of the Twin Creeks mine are gas poor with total concentrations of 0.2–3.4 mol% (Fig. 11).

There is also a difference in dominant gas species for the different fault zones, and mines. At the Getchell mine, all samples from NE-trending faults have CO_2 as the dominant gas specie with maximum N_2 concentrations of 0.8 mol% (Fig. 12a). In contrast, N-trending faults contain appreciable amounts of N_2 (up to 1.6 mol%) relative to CO_2 in some samples (Fig. 12b). This relationship is more pronounced at the Twin Creeks mine, where N_2 and CO_2 concentrations can be equal at total gas concentrations ≤0.5 mol% (Fig. 12c). Fluid inclusions in samples of Main-stage jasperoid at the Twin Creeks mine contain N_2 as the principal gas with concentrations up to 7.9 mol% (Groff, 2018b).

Fluid inclusions in paragenetically younger realgar and quartz are gas poor (Appendix 1). Realgar separated from samples at the

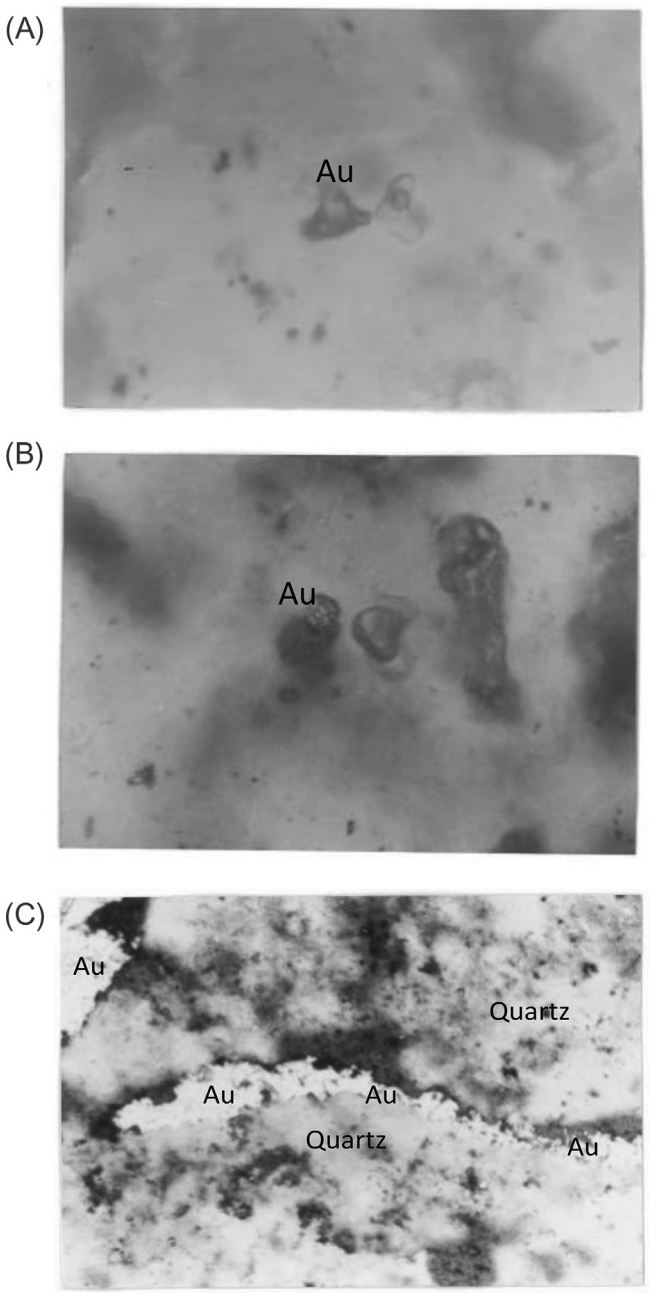

Fig. 6. Photomicrographs of quartz with (a) a liquid- rich fluid inclusion (~7 μm) to the right of a grain of native gold and b) a vapor-rich inclusion (~8 μm) to the right of a grain of native gold in sample DZADUL (Table 1), Twin Creeks mine. A larger all vapor (?) inclusion is to the right of the vapor-rich inclusion. C) A discontinuous band of native gold (~2 mm) at the center of the field of view, oriented right–left, between quartz grains containing cogenetic vapor-rich and liquid-rich inclusions. Intergrown with the quartz is 42 Ma adularia.

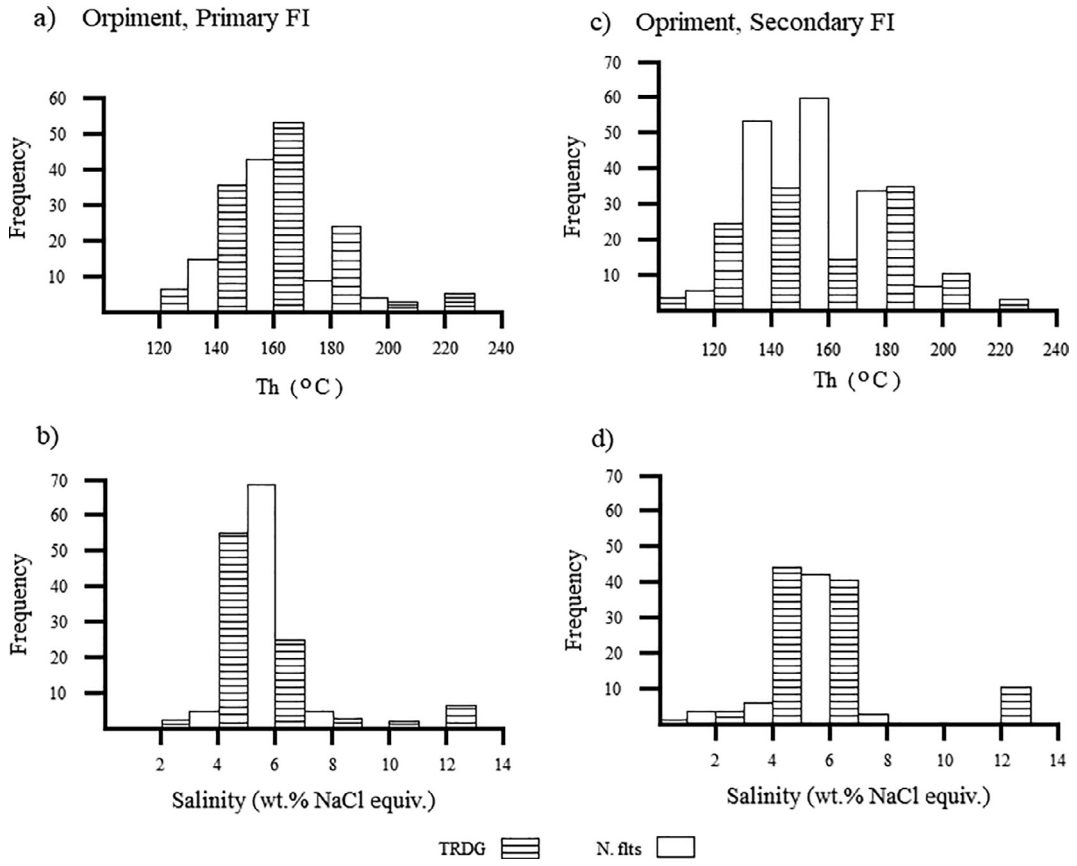

Fig. 7. Histograms of T_h and salinity data for primary and secondary fluid inclusions in orpiment samples from the Getchell mine. Abbreviations: TRDG = the NE-trending Turquoise Ridge Fault and N. flts = N-trending faults.

intersection of N- and NE-trending faults, Getchell mine contains inclusions with total gas contents of 0.2–0.7 mol%. Inclusions in quartz, containing disseminated native gold and intergrown with 42 Ma adularia, have total gas contents of 0.4–1.8 mol%.

4.4. Depth estimates

Boiling point curves were used to estimate depths, assuming hydrostatic conditions, for Eocene quartz–adularia–gold and orpiment mineralization due to fluid inclusion evidence of boiling and the absence of CO_2-rich inclusions. Hydrothermal solutions that deposited native gold in epithermal veins had total gas contents of 0.4–1.8 mol% (Appendix 1) and T_h of 206–330 °C (Fig. 9). Due to the range in Th data and inability to observe ice melting in inclusions ≤ 8 μm in size, boiling conditions are based on temperatures of 240–280 °C and assumed salinities ≤ 5 wt% NaCl equiv. that are similar to Late-stage Carlin type mineralization. These data yield depths of 480–980 m (Fig. 13a).

Primary liquid-rich and vapor-rich fluid inclusions hosted by orpiment homogenize to the liquid and vapor phases, respectively, at temperatures of 173–203 °C. These temperatures, salinities of 4–6 wt% NaCl equiv., and QMS analyses that record total gas contents ≤ 4.6 mol % yield depths of 110–250 m for boiling (Fig. 13b) during Late-stage Carlin-type mineralization.

5. Discussion

5.1. Mechanism(s) of boiling

Assemblages of cogenetic vapor-rich and liquid-rich inclusions (Figs. 3a, b, and 4c) that are indicative of boiling (Roedder, 1984) were only identified in samples from NE-trending faults or structural intersections involving these faults. Although T_h of vapor-rich inclusions in orpiment are limited due to decrepitation, there is a close correspondence with T_h of liquid-rich inclusions in the same field of view that define a range of 173–203 °C. Primary vapor-rich inclusions did not form by necking down based on their distribution, shape, and size (Fig. 3a). If leakage had occurred it would have affected all inclusions in the same way, yet samples of banded calcite contain distinct populations in mottled and clear bands.

The significant differences in total gas contents of fluid inclusions in orpiment and realgar also support boiling (Appendix 1). Orpiment samples from N-trending faults that contain only liquid-rich inclusions have total gas contents ≤ 4.6 mol%, compared with total gas contents up to 12.1 mol% for orpiment hosting cogenetic vapor-rich and liquid-rich inclusions from NE-trending faults and structural intersections (Fig. 10). One-phase liquid inclusions in realgar contain < 1 mol% total gas.

The boiling of hydrothermal solutions can result by fluid mixing and tectonic decompression (Roedder, 1984). Stable isotope data indicate mixing between a magmatic fluid and meteoric water during Late-stage mineralization (Groff, 2018a,b). Relevant to the present study, orpiment (sample 92–225) and banded calcite (sample 99–1550) have δD values of −57‰ and −103‰, respectively. The distribution of data in T_h vs. salinity plots of primary and secondary inclusions in orpiment also supports mixing (Fig. 14). Furthermore, gas data record different compositions with samples from NE-trending faults containing CO_2 as the dominant specie and elevated levels of C_nH_m (Figs. 12 and 15).

Although fluid mixing did occur in the Getchell deposit, boiling likely resulted when magmatic fluids were injected into NE-trending faults that had been sealed by Main-stage silicification, and subsequently ruptured. Fluid inclusions with the highest gas contents are in crosscutting orpiment veins or the matrix to breccia surrounding clasts

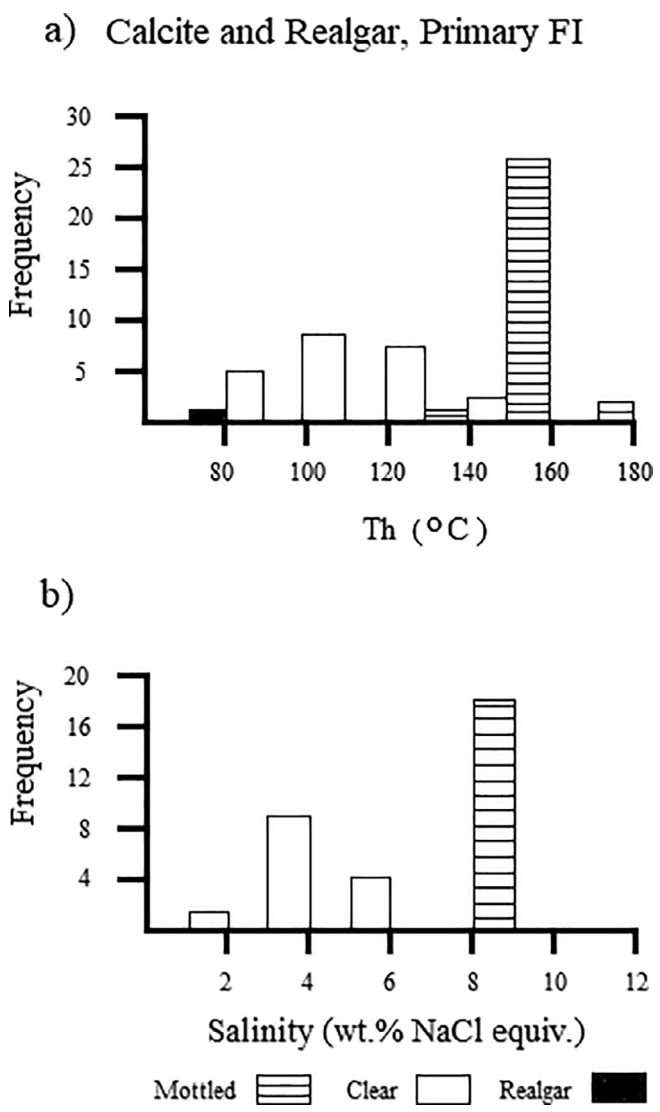

Fig. 8. Histograms of T_h and salinity data for primary fluid inclusions in banded calcite and realgar, Getchell mine.

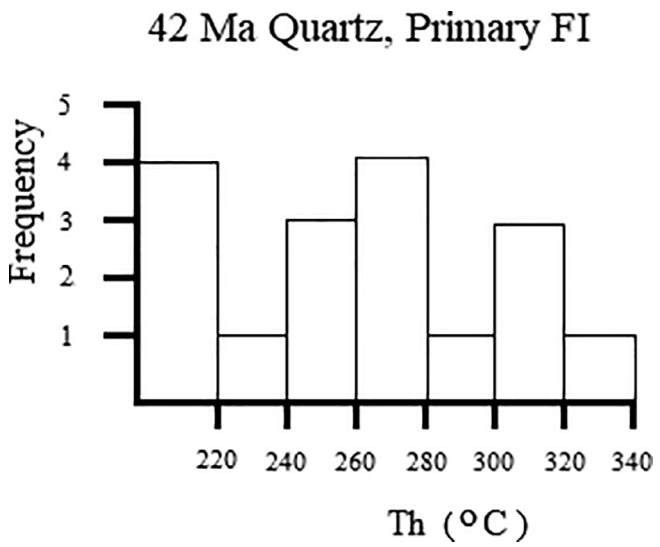

Fig. 9. Histogram of T_h data for primary fluid inclusions in a quartz–adularia–gold vein, Twin Creeks mine.

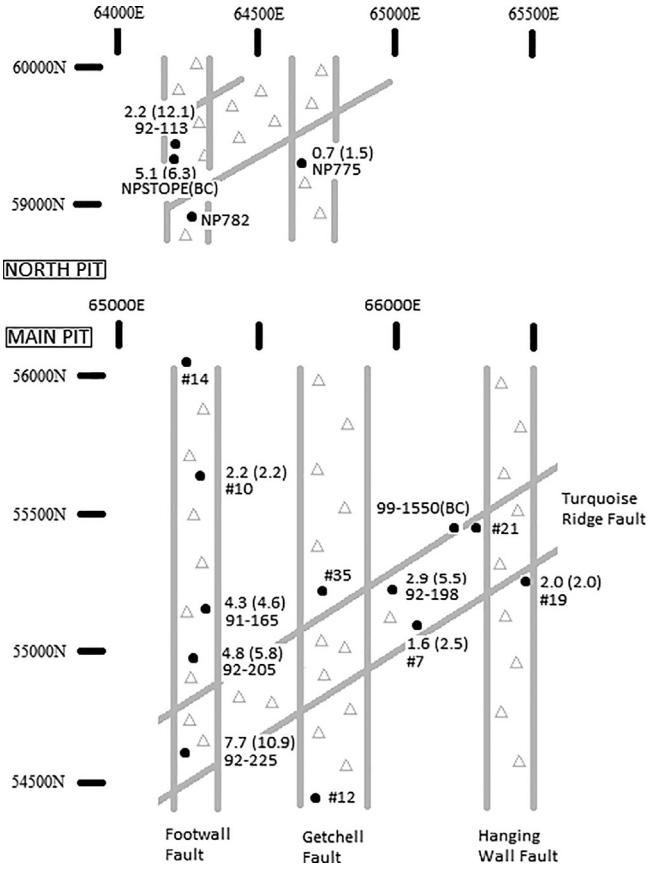

Fig. 10. A plan view of the Main and North pits, Getchell mine showing the position of orpiment and banded calcite samples relative to different faults. (BC) = samples of banded calcite; average and maximum values of gas analyses are indicated by 7.7 (10.9), respectively.

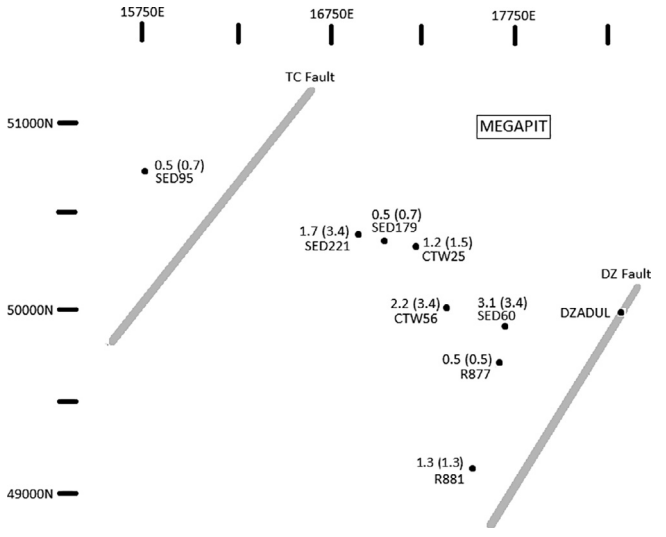

Fig. 11. A plan view of part of the Mega pit, Twin Creeks mine showing the location of orpiment samples and the 42 Ma quartz vein (DZADUL) relative to NE-trending faults. Average and maximum values of gas analyses are indicated by 1.7 (3.4), respectively.

of jasperoid ore that occur at the intersection of the N-trending Footwall Fault and NE-trending faults. In contrast, dissolution cavities and open fractures are lined by orpiment crystals containing gas-poor inclusions. At the Twin Creeks mine, samples of bedding replacement ore between NE-trending faults also contain open-space fillings of orpiment crystals,

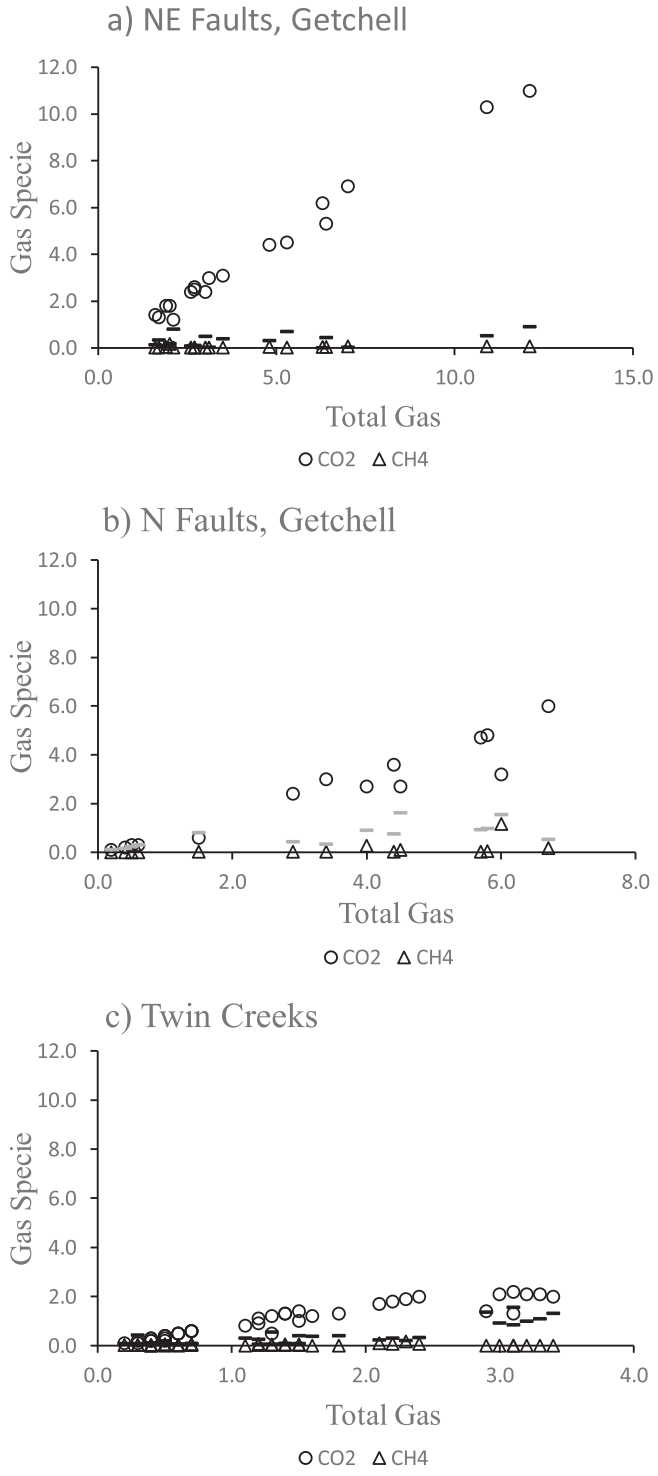

Fig.12. Plots of gas concentrations for individual gas species (e.g., N_2, CO_2, CH_4) vs. the total gas content of fluid inclusions in orpiment from the Getchell and Twin Creeks mines. Note that scales for the x-axis are different and all QMS gas data are reported in mol%. Abbreviations: N = N-trending faults and NE = NE-trending faults.

which host gas-poor inclusions (Fig. 11). The QMS gas data of orpiment from Twin Creeks are most similar to orpiment crystals sampled beyond structural intersections and in N-trending faults at the Getchell mine. These relationships support boiling related to tectonic decompression of NE-trending faults, followed by fluid mixing in open fractures of surrounding rocks.

Boiling is not proposed as a mechanism for gold deposition as in

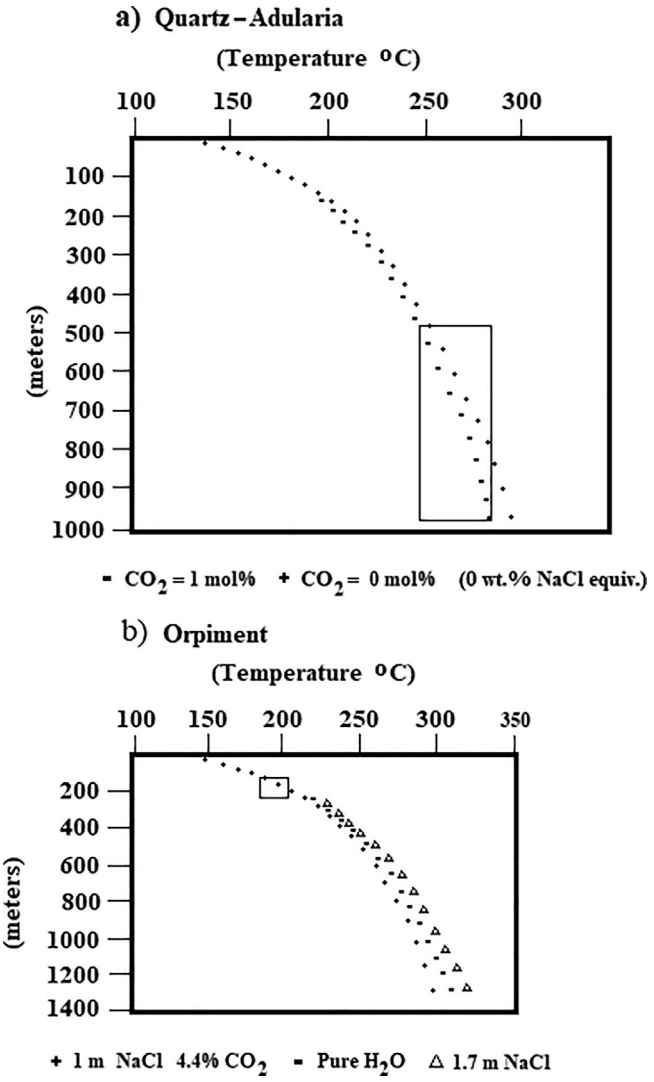

Fig. 13. Boiling point curves for a) the system H_2O–CO_2 used to determine depths for quartz–adularia–gold mineralization and b) the system H_2O–NaCl–CO_2 used to determine depths for orpiment mineralization. The boxed areas represent conditions during epithermal vein and Carlin-type mineralization. Data in the boiling point curves are from Drummond and Ohmotto (1985) and Wilkinson (2001).

epithermal deposits (Drummond and Ohmotto, 1985) due to the fundamental role that sulfidation played in the formation of Carlin-type gold deposits. However, the deposition of native gold in the 42 Ma quartz–adularia vein, Twin Creeks mine may have occurred due to boiling. As shown in Section 4.1, there were multiple events of native gold deposition and boiling is indicated by cogenetic liquid-rich and vapor-rich inclusions. Other epithermal characteristics of these high-grade veins include quartz–adularia alteration, fluid inclusions with T_h of 206–330 °C, structural control of mineralization, ore grades that decrease with depth, and δD of –64 per mil for quartz (Groff, 1996).

5.2. CO_2-rich fluid inclusions, an artifact of boiling

The fact that no CO_2-rich inclusions were identified in samples of orpiment–realgar–calcite–barite mineralization from the Getchell, Twin Creeks, Betze, and Carlin mines by Radtke et al. (1980), Groff (1996), and Groff et al. (2002) or reported in subsequent literature indicates that CO_2-rich inclusions are not characteristic of Late-stage mineralization. Yet Cline and Hofstra (2000) identified CO_2-rich secondary fluid inclusions in purple fluorite from the North pit, Getchell mine and

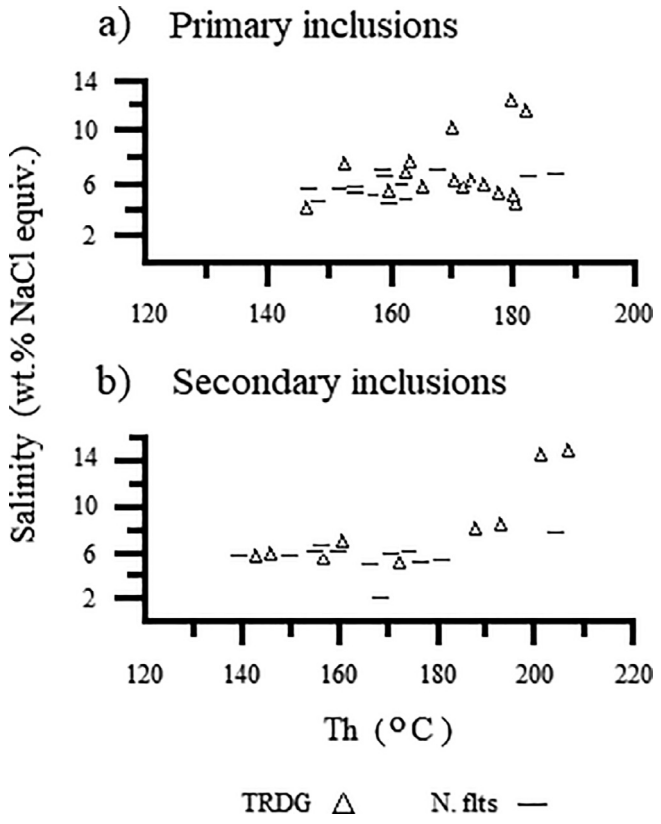

Fig. 14. Plots of T_h vs. Salinity for orpiment from the Getchell mine. Abbreviations: TRDG = the NE-trending Turquoise Ridge Fault and N flts = N-trending faults.

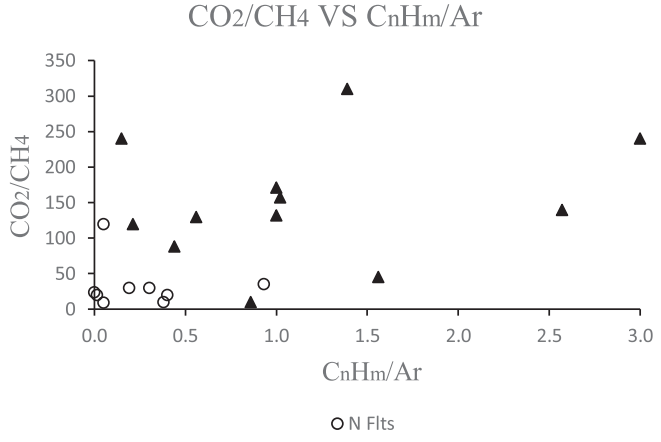

Fig. 15. Plot of CO_2/CH_4 vs. C_nH_m/Ar for orpiment samples from the Getchell mine. Abbreviations: N = N-trending faults and NE = NE-trending faults.

used the microthermometric data to calculate pressures ≥330 bars and depths > 1.2 km. An ore sample from the TRDG deposit containing fluorite mantled by a thin layer of pyrite and surrounded by orpiment documents the mineral paragenesis (Shigehiro, 1999).

As fluorite is a rare mineral in Carlin-type deposits, where it occurs at the Getchell mine has significance. Occurrences of fluorite are limited to a NE-trending structure in the North pit and centered on the NE-trending TRDG Fault (Groff et al., 1997; Shigehiro, 1999). These are the same localities where cogenetic vapor-rich and liquid-rich fluid inclusions exist in orpiment and banded calcite, which suggests an association with boiling.

An analogy is provided by fluid inclusion studies of a single quartz crystal that document changing P–T–X conditions with time in the Broadlands–Ohaaki geothermal system, New Zealand (Simmons et al., 2007). Inclusions in the crystal core have CO_2 concentrations of 7.9–14.3 mole% and T_h of 291 °C to > 365 °C, whereas CO_2-poor inclusions in a quartz overgrowth have T_h of ~300 °C. The periodic sealing of permeable channels due to mineral precipitation, overpressuring of the system, and subsequent rupture resulted in boiling. Different types of fluid inclusions in orpiment (Fig. 3), banded calcite (Fig. 4), and realgar (Fig. 5) at the Getchell mine record a similar process.

Shallow depths of mineralization in Carlin-type deposits of Nevada are supported by more-recent studies and textures of igneous rocks. The Alligator Ridge deposit formed at depths of ≤300 m to 800 m based on an Eocene reconstruction, fluid inclusion data, and the presence of amorphous silica that is a precursor to jasperoid (Nutt and Hofstra, 2003). Hickey et al. (2003) used thermal modeling of apatite to conclude that the northern Carlin trend had cooled to < 60 °C by the Eocene and mineralization occurred at depths as shallow as 800 m. This is supported by devitrification textures in dikes at the Jerritt Canyon mine and glassy selvages in mineralized Deep Star rhyolite (Cline et al., 2005).

At the Twin Creeks mine, Carlin-type ore and crosscutting epithermal veins, which formed at depths of 480–980 m, have precise adularia ages that are indistinguishable within analytical uncertainty. Such a rapid transition between different mineralizing systems is possible because apatite fission-track ages and thermal modeling of Mainstage mineralization in the Betze–Post deposit, Carlin trend indicates a maximum duration of < 15 Ka to 45 Ka for hydrothermal fluid flow (Hickey et al., 2014). Short-lived gold events in the Getchell trend were documented by Barker et al. (2009) through Nanosims analyses of pyrite from the Turquoise Ridge deposit that identified distinct textures and chemical zoning.

As the 42 Ma quartz–adularia–native gold mineralization that cuts jasperoid ore at the Twin Creeks mine represents a distinct event, this can explain the rarity of adularia in Carlin-type deposits.

6. Conclusions

Boiling occurred in NE-trending faults during the later stages of Eocene Carlin-type gold mineralization at the Getchell and Twin Creeks mines. Continuous boiling during the formation of orpiment at the Getchell mine became episodic in paragenetically younger banded calcite that contains realgar. At Twin Creeks, boiling is restricted to the NE-trending DZ Fault. Depths of ≤980 m, assuming hydrostatic conditions, are indicated for Eocene gold mineralization in the Getchell trend. The 42 Ma quartz-adularia-pyrite-gold vein at Twin Creeks shows that Carlin-type gold deposits can contain epithermal veins that are easy to date. Such veins maybe present in other Carlin-type gold deposits of Nevada and Carlin-style gold deposits in other parts of the world.

Acknowledgments

The author would like to thank Mr. Richard Nanna (Getchell Gold Corp) and Mr. Dean Peltonen (Santa Fe Pacific Gold Corp) for supporting the study through assistance with sample collection and funding of fluid inclusion analyses. Discussions of the fluid inclusion microthermometry and gas analyses with the late Dr. David Norman proved valuable in interpreting the data. The constructive comments and suggestions made by Dr. Albert Hofstra and an anonymous reviewer also improved the manuscript.

Appendix 1

Quadrupole mass spectrometer gas data (mol%) of orpiment, realgar, and quartz samples from the Getchell (G) and Twin Creeks (TC) mines

Sample ID	Mineral	H2O	Total Gas	CO2	CH4	N2	CnHm (×100)	Ar (×100)
(G)NP775	Orpiment	99.5	0.5	0.3	0.01	0.23	0.06	0.2
		99.6	0.4	0.2	0.01	0.16	0.06	0.15
		98.5	1.5	0.6	0.03	0.79	0.01	0.79
		99.4	0.6	0.3	0.01	0.30	0.06	0.31
		99.8	0.2	0.1	0.01	0.09	0.03	0.08
(G)92-225	Orpiment	93.6	6.4	5.3	0.04	0.43	0.49	0.49
		89.1	10.9	10.3	0.06	0.50	0.40	0.4
		95.2	4.8	4.4	0.05	0.31	0.16	0.36
(G)91-165	Orpiment	95.5	4.5	2.7	0.11	1.60	0.04	1.71
		96	4.0	2.7	0.28	0.89	0.05	0.94
(G)92-198	Orpiment	97.1	2.9	2.4	0.02	0.43	0.02	0.41
		93.3	6.7	6.0	0.17	0.51	0.50	0.54
		94	6.0	5.2	0.17	0.53	0.64	0
(G)#7	Orpiment	98.3	1.7	1.3	0.01	0.33	0.14	0.25
		98	2.0	1.8	0.17	0.17	0.18	0.21
		97.4	2.6	2.4	0.01	0.08	0.21	0.07
		98.4	1.6	1.4	0.01	0.13	0.18	0.07
		96.5	3.5	3.1	0.01	0.39	0.25	0.18
		96.9	3.1	3.0	0.02	0.02	0.23	0.04
(G)92-113	Orpiment	87.9	12.1	11.0	0.07	0.90	0.55	0.54
		94.7	5.3	4.5	0.01	0.68	0.12	0.73
		97	3.0	2.4	0.01	0.49	0.09	0.62
		97.9	2.1	1.2	0.01	0.80	0.26	1.23
(G)#19	Orpiment	98.1	1.9	1.8	0.04	0.06	0.14	0.09
(G)#10	Orpiment	97.8	2.2	2.1	0.03	0.01	0.09	0.07
(G)92-205	Orpiment	96.6	3.4	3.0	0.03	0.32	0.15	0.43
		95.6	4.4	3.6	0.03	0.74	0.00	0.39
		94.3	5.7	4.7	0.03	0.91	0.00	0.29
		94.2	5.8	4.8	0.04	0.96	0.00	0.41
(G)NPSTOPE	Orpiment	97.3	2.7	2.6	0.02	0.08	0.27	0
		97.4	2.7	2.5	0.02	0.10	0.28	0
		93.7	6.3	6.2	0.04	0.00	0.53	0
		93	7.0	6.9	0.06	0.01	0.65	0
(TC)SED221	Orpiment	96.7	3.3	2.1	0.01	1.09	0.10	1.27
		98.4	1.6	1.2	0.00	0.37	0.04	0.38
		98.2	1.8	1.3	0.00	0.40	0.06	0.38
(TC)SED60	Orpiment	97.1	2.9	1.4	0.00	1.36	0.06	1.23
		96.9	3.1	1.3	0.00	1.55	0.04	1.38
		96.56	3.4	2.0	0.00	1.31	0.00	1.24
		96.82	3.2	2.1	0.01	0.99	0.00	0.92
		96.9	3.1	2.2	0.01	0.83	0.06	0.84
		97	3.0	2.1	0.01	0.90	0.05	0.77
(TC)SED179	Orpiment	99.6	0.4	0.3	0.00	0.04	0.01	0.04
		99.7	0.4	0.3	0.01	0.03	0.01	0.03
		99.5	0.5	0.4	0.01	0.03	0.00	0.03
		99.3	0.7	0.6	0.02	0.07	0.01	0.08
		99.4	0.6	0.5	0.01	0.02	0.01	0.03
		99.4	0.6	0.5	0.02	0.04	0.01	0.04
(TC)R769	Orpiment	98.6	1.4	1.3	0.05	0.07	0.05	0.05
		98.6	1.4	1.3	0.03	0.07	0.07	0.04
		98.8	1.3	1.2	0.04	0.06	0.05	0.04
		98.7	1.5	1.4	0.04	0.07	0.05	0.03
		98.5	1.2	1.1	0.03	0.05	0.05	0.03
(TC)CTW25	Orpiment	98.5	1.5	1.0	0.02	0.39	0.14	0.37
		98.9	1.1	0.8	0.01	0.30	0.10	0.28
		98.8	1.2	0.9	0.08	0.24	0.17	0.17
(TC)R765	Orpiment	99.5	0.5	0.3	0.02	0.18	0.03	0.32
		99.8	0.2	0.1	0.02	0.07	0.03	0.09
		99.7	0.3	0.1	0.01	0.42	0.03	0.15
		99.6	0.4	0.2	0.02	0.11	0.04	0.12
		99.7	0.3	0.2	0.02	0.07	0.04	0.08
		99.6	0.4	0.2	0.03	0.10	0.05	0.11
(TC)SED95	Orpiment	99.5	0.5	0.4	0.02	0.08	0.04	0.09
		99.5	0.5	0.4	0.05	0.11	0.04	0.11
		99.3	0.7	0.6	0.05	0.08	0.05	0.08
		99.3	0.7	0.6	0.04	0.05	0.06	0.06
		99.3	0.7	0.6	0.04	0.04	0.06	0.05
		99.4	0.6	0.5	0.03	0.05	0.04	0.07
(TC)CTW56	Orpiment	97.7	2.3	1.9	0.18	0.20	0.06	0.13
		97.9	2.1	1.7	0.09	0.23	0.07	0.19
		97.8	2.2	1.8	0.06	0.30	0.08	0.18

(*continued on next page*)

Quadrupole mass spectrometer gas data (mol%) of orpiment, realgar, and quartz samples from the Getchell (G) and Twin Creeks (TC) mines (*continued*)

Sample ID	Mineral	H2O	Total Gas	CO2	CH4	N2	CnHm (×100)	Ar (×100)
		97.6	2.4	2.0	0.06	0.32	0.07	0.38
(TC)R881	Orpiment	99.5	0.5	0.2	0.04	0.16	0.19	0.09
(TC)R877	Orpiment	98.7	1.3	0.5	0.03	0.53	0.44	0.18
(G)92-225	Realgar	99.4	0.6	0.4	0.02	0.21	0.04	0.18
		99.7	0.3	0.2	0.03	0.02	0.04	0.02
		99.4	0.6	0.5	0.04	0.04	0.06	0.04
		99.4	0.6	0.5	0.04	0.04	0.06	0.03
		99.4	0.6	0.6	0.04	0.06	0.05	0.05
(G)NPSTOPE	Realgar	99.3	0.7	0.5	0.04	0.09	0.035	0.04
		99.5	0.5	0.4	0.02	0.03	0.01	0.02
		99.7	0.3	0.2	0.02	0.04	0.02	0.03
		99.6	0.4	0.3	0.02	0.04	0.03	0.00
		99.6	0.4	0.4	0.02	0.05	0.04	0.02
		99.6	0.4	0.3	0.03	0.04	0.05	0.02
(TC)DZADUL	Quartz	98.2	1.8	1.6	0.13	0.00	0.03	0
		99.2	0.8	0.6	0.12	0.08	0.05	0.01
		99.6	0.4	0.3	0.07	0.02	0.01	0.02
		99.4	0.6	0.4	0.09	0.08	0.04	0.02
		99.5	0.5	0.4	0.08	0.03	0.03	0.004

Appendix A. Supplementary data

Supplementary data to this article can be found online at https://doi.org/10.1016/j.oregeorev.2019.02.013.

References

Barker, S.L.L., Hickey, K.A., Cline, J.S., Dipple, G.M., Kilburn, M.R., Vaughan, J.R., Longo, A.A., 2009. Uncloaking invisible gold: use of nanosims to evaluate gold, trace elements, and sulfur isotopes in pyrite from carlin-type deposits. Econ. Geol. 104, 897–904.

Brown, K.C., 1986. Gold deposition from geothermal discharges in New Zealand. Econ. Geol. 81, 979–983.

Chevillon, V., Berensen, E., Gingrich, M., Howard, W., Zbinden, E., 2000. Geologic overview of the Getchell Gold Mine Geology. Soc. Econ Geol. Guidebook Series 32, 195–205.

Cline, J.S., 2001. The timing of gold and arsenic sulfide mineral deposition at the getchell carlin-type gold deposit, North-Central Nevada. Econ. Geol. 96, 75–95.

Cline, J.S., Hofstra, A.H., 2000. Ore fluid evolution at the Getchell Carlin-type gold deposit, Nevada, USA. Eur. J. Mineral. 12, 195–212.

Cline, J.S., Hofstra, A.H., Muntean, J.L., Tosdale, R.M., Hickey, K.A., 2005. Carlin-type gold deposits in Nevada: critical geologic characteristics and viable models. Econ. Geol. 100th Anniv. Vol, 451–484.

Drummond, S.E., Ohmotto, H., 1985. Chemical evolution and mineral deposition in boiling hydrothermal systems. Econ. Geol. 80, 126–147.

Fortuna, J., Kesler, S.E., Stenger, D.P., 2003. Source of Iron for sulfidation and gold deposition, twin creeks carlin-type deposit, Nevada. Econ. Geol. 98, 1213–1224.

Groff, J.A., 1996. $^{40}Ar/^{39}Ar$ geochronology of gold mineralization and origin of auriferous fluids for the getchell and twin creeks mines, Humboldt County, Nevada. Unpub. PhD thesis. Institute of Mining and Technology, Socorro, New Mexico, pp. 291.

Groff, J.A., 2018a. Fluid mixing during late-stage carlin-type mineralization in the getchell and twin creeks deposits, Nevada, United States. Ore Geol. Rev. 960–965.

Groff, J.A., 2018b. Distinguishing generations of quartz and a distinct gas signature of deep high-grade Carlin-type gold mineralization using quadrupole mass spectrometry. Ore Geol. Rev. 95, 518–536.

Groff, J.A., Heizler, M.T., McIntosh, W.C., Norman, D.I., 1997. $^{40}Ar/^{39}Ar$ dating and mineral paragenesis for carlin-type gold deposits along the getchell trend, nevada: evidence for cretaceous and tertiary gold mineralization. Econ. Geol. 92, 601–622.

Groff, J.A., Campbell, A.R., Norman, D.I., 2002. An evaluation of fluid inclusion microthermometric data for orpiment–realgar–calcite–barite–gold mineralization at the Betze and Carlin Mines, Nevada. Econ. Geol. 97, 1341–1346.

Hall, C.M., Kesler, S.E., Simon, G., Fortuna, J., 2000. Overlapping cretaceous and eocene alteration, twin creeks carlin-type deposit, Nevada. Econ. Geol. 95, 1739–1752.

Hedenquist, J.W., Arribas, R.A., Gonzales-Urien, E., 2000. Exploration for epithermal gold deposits. Rev. Econ. Geol. 13, 245–277.

Hickey, K.A., Donelick, R.A., Tosdal, R.M., McInnes, B.I.A., 2003. Restoration of the Eocene landscape in the Carlin-Jerritt canyon mining district: constraining depth of mineralisation for carlin-type au-deposits using low-temperature apatite thermochronology [abs.]. Geol. Soc. Am. Abstr. Prog. 35 (6), 358.

Hickey, K.A., Barker, L.L., Dipple, G.M., Arehart, G.B., Donelick, R.A., 2014. The brevity of hydrothermal fluid flow revealed by thermal halos around giant gold deposits: implications for carlin-type gold systems. Econ. Geol. 109, 1461–1487.

Hofstra, A.H., Cline, J.S., 2000. Characteristics and models for carlin-type gold deposits. Rev. Econ. Geol. 13, 163–220.

Hofstra, A.H., Premo, W.R., Emsbo, P., Cline, J.S., Aleinikoff, J.N., 2000. U–Th–Pb dating of hydrothermal minerals from carlin-type gold deposits: results and evaluation. In: Cluer, J.K., Price, J.G., Strushsacker, E.M., Hardyman, R.F., Morris, S.L. (Eds.), Geology and Ore Deposits 2000: The Great Basin and Beyond: Symposium Proceedings. Geological Society of Nevada, Reno, pp. 61–77.

Lubben, J., 2004. Unpub. MSc thesis In: Quartz as Clues to Paragenesis and Fluid Properties at the Betze-Post Deposit, Northern Carlin Trend, Nevada. Univ. of Nevada, Las Vegas, pp. 155p.

Madden-McGuire, D.J., Marsh, S.P., 1991. Lower Paleozoic host rocks in the getchell gold belt: several distinct Allochthons or a sequence of continuous sedimentation? Geology 19, 489–492.

Norman, D.I., Moore, J.N., Yonaka, B., Musgrave, J., 1996. Gas Species in Fluid Inclusions: A Tracer of Fluids and Indicator of Fluid Processes: Symposium Proceedings, Twenty-First Workshop on Geothermal Reservoir Engineering. Stanford. Univ Stanford, California, pp. 233–240.

Nutt, C.J., Hofstra, A.H., 2003. A Shallow Carlin-type Gold District:Econ. Geol. 98, 1225–1241.

Osterberg, M.W., 1990. Unpub. PhD thesis In: Geology and Geochemistry of the Chimney Creek Gold Deposits, Humboldt County, Nevada. Univ. of Arizona, Tucson, pp. 173.

Radtke, A.S., Rye, R.O., Dickson, F.W., 1980. Geology and stable isotope studies of the carlin gold deposit, Nevada. Econ. Geol. 75, 641–672.

Roedder, E., 1984. Fluid inclusions. Rev. Mineral 12, 646p.

Shigehiro, M., 1999. Mineral Paragenesis and Ore Fluids at the Turquoise Ridge Gold Deposit, Nevada. Unpub. MSc thesis. Univ. of Nevada, Las Vegas, pp. 152p.

Simmons, S.F., Simpson, M.P., Reynolds, T.J., 2007. The significance of clathrates in fluid inclusions and the evidence for overpressuring in the broadlands-Ohaaki geothermal system, New Zealand. Econ. Geol. 102, 127–135.

Stenger, D.P., Kesler, S.E., Peltonen, D.R., Tapper, C.J., 1998. Deposition of gold in carlin-type deposits; the role of sulfidation and decarbonation at twin creeks, Nevada. Econ. Geol. 93, 201–215.

Tretbar, D., Arehart, G.B., Christensen, J.N., 2000. Dating gold deposition in a carlin-type gold deposit using Rb/Sr methods on the mineral Galkhaite. Geology 28, 947–950.

Wilkinson, J.J., 2001. Fluid inclusions in hydrothermal ore deposits. Lithos 55, 229–272.